Synthesis, Structure, and Optical Activity of HPM-1, a Pure Silica Chiral Zeolite

Alex Rojas,[†,‖] Oriol Arteaga,[‡,§] Bart Kahr,[‡] and Miguel A. Camblor*,[†]

[†]Instituto de Ciencia de Materiales de Madrid (ICMM), Consejo Superior de Investigaciones Científicas (CSIC), Sor Juana Inés de la Cruz 3, 28039 Madrid, Spain

[‡]Department of Chemistry, New York University, New York, New York 10003, United States

[§]Departament de Física Aplicada i Òptica, Universitat de Barcelona, 08028-Barcelona, Spain

Ⓢ Supporting Information

ABSTRACT: 2-Ethyl-1,3,4-trimethylimidazolium is a poor organic structure-directing agent in the synthesis of pure silica zeolites using fluoride as a mineralizer at 150 °C. Under these conditions only ill-crystallized solids are obtained after long hydrothermal treatments (several weeks). It disappoints despite its relatively large size, conformational rigidity, and intermediate hydrophilic/hydrophobic character, attributes which would qualify it as a promising structure-directing agent, according to prior investigations. By raising the crystallization temperature to 175 °C under otherwise identical conditions, crystallization is dramatically accelerated. Depending on the water/silica ratio and crystallization time, two different materials are obtained: the recently reported pure silica polymorph of the chiral STW-type zeolite, HPM-1, and the new layered organosilicate, HPM-2. Prolonged heating transforms these phases into the small-pore ITW-type zeolite, while no signs of the SOF-type zeolite (formally built from the same layers as STW) was found. A complete physicochemical and structural characterization of the as-made chiral HPM-1 zeolite is provided, and the proposed stabilization of this zeolite by polarization of the Si−O bond is supported by the observed deviation from tetrahedrality. HPM-1 is optically active, and a study of several crystallites by Mueller matrix microscopy shows that their optical activity can be individually measured and that this technique could be useful for the assessment of the enantiomeric purity of a microcrystalline powder.
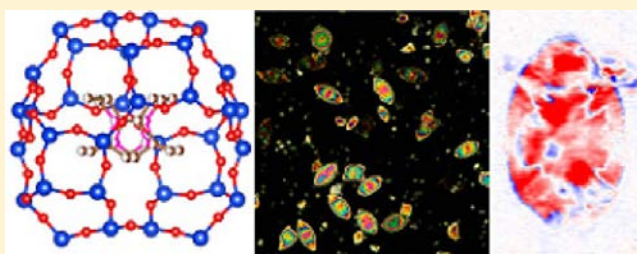
INTRODUCTION

Since the report in 1988 of the structure of zeolite β,[1] a complex intergrowth of several polymorphs, one of them chiral, the possibility of using zeolites in enantioselective processes became an attractive possibility. Some chiral zeolites and zeolite-like materials actually exist in pure form,[2] but the efficient application to enantioselective processes requires also that the material impose strong enantioselective interactions at a molecular level. Some limited success was claimed in a review, where a zeolite β was synthesized with a chiral organic structure-directing agent (SDA).The resulting material showed moderate enantiomeric excess (ee ≈ 5%) in the acid hydrolysis of *trans*-stilbene oxide as well as in the selective adsorption of the resulting diols.[3] However, this preliminary report was not followed by a comprehensive description of the synthesis, catalysis, and separation processes. Dryzun et al. have also demonstrated significant enantioselective adsorption of amino acids on natural, chiral zeolites by calorimetry. This was achieved not through crystallographic resolution but by grinding a single crystal of just one enantiomorph.[2]

The recent discovery of HPM-1,[4] a pure silica zeolite possessing the chiral STW-type zeolite structure, looks promising with respect to potential applications (zeolite framework types are designated by three-letter codes, such as

STW, which uniquely define the connectivity of the tetrahedra from which zeolites are built).[5] First, HPM-1 possesses a helical pore in which enantiomeric restrictions at a molecular level may be envisaged. Second, unlike the germanosilicate zeolite SU-32 that first presented the STW structure and which constitutes its "type material",[6] HPM-1 displays the large thermal and hydrothermal stability characteristic of silica-based zeolites.

Here, we report a comprehensive study of the synthesis of HPM-1 using 2-ethyl-1,3,4-trimethylimidazolium (2E134TMI) and fluoride as structure-directing agents, as well as its detailed structural and physicochemical characterization. Of particular interest is that the initial experiments at 150 °C (a temperature that can be considered as "standard" in zeolite synthesis) essentially failed. At 175 °C, the crystal chemistry was much richer. Structure direction in this system is discussed, and we give experimental evidence for a significant deformation of the silica framework, supporting the idea that host−guest interactions enhance framework flexibility in STW and allow its crystallization. Finally, measurements of the optical activity of HPM-1 by Mueller matrix polarimetry are used to distinguish enantiomorphous crystallites. Characterizing the

circular birefringence of anisotropic microcrystals, while challenging, is in principle a realizable method for monitoring enantioselectivity of chiral zeolite synthesis.

■ EXPERIMENTAL SECTION

Synthesis of the Organic Cation. 2E134TMI was obtained in iodide form by methylation at both N positions of 2-ethyl-4-methylimidazole (0.08 mol, Aldrich, 95%) in chloroform (100 mL, Carlo Erba, synthesis grade) using methyl iodide (0.16 mol) in the presence of potassium carbonate sesquihydrate (Aldrich, 99%). After stirring for 2 days at room temperature, followed by a second addition of methyl iodide (0.16 mol) and stirring for 4 days, the mixture was filtered and the solid washed with chloroform. The desired salt was obtained by rotary evaporation of the organic solution under vacuum. (*Caution! Toxic vapors evolve. Use a trap and work under a fume hood.*) Chemical analysis (found, 35.91% C, 5.53% H, 10.52% N; expected for $C_8H_{15}N_2I$, 36.10% C, 5.68% H, 10.53% N) and ^1H and ^{13}C NMR in solution (see below) confirmed that the product synthesized was 2E134TMII. The iodide was then converted to the hydroxide form by anion exchange using Dowex monosphere 550A (OH) anion exchange resin. The hydroxide solutions were concentrated by rotary evaporation to around 1−1.5 mol/1000 g. The final hydroxide concentration was determined by titration with phenolphthalein indicator.

Zeolite Synthesis. Tetraethyl orthosilicate was hydrolyzed under magnetic stirring at room temperature in an aqueous solution of the hydroxide form of the organic cation. All the ethanol produced in the hydrolysis, and some water, was allowed to evaporate, and stirring was stopped when the desired composition was achieved. The amount of water evaporated was monitored by weight. Finally, HF (ca. 48%, Aldrich, recently titrated) was added while the mixture was stirred with a spatula for 15 min. The crystallization was carried out at 150, 175, or 185 °C in Teflon vessels inside stainless steel autoclaves that were tumbled at about 60 rpm. At different intervals of time, the autoclaves were taken out of the oven and the solid product was recovered, washed with ample amounts of deionized water, and dried at 100 °C. The final composition of the reaction mixtures was SiO_2:0.5-(2E134TMIOH):0.5HF:xH$_2$O, and the water to silica ratio, x, was varied between 3.3 and 10.

Characterization. Products were identified by powder X-ray diffraction (XRD; Bruker D8 Advance diffractometer, Cu Kα radiation, 5−45° 2θ range). Multinuclear magic angle spinning nuclear magnetic resonance spectra (^{19}F, ^{13}C, and ^{29}Si MAS NMR) were recorded on a Bruker AV 400WB, and details are given elsewhere.[7] Thermogravimetric analyses were made with an SDT Q600 TA Instruments device which reaches 1000 °C (heating rate 10 °C/min, oxygen flow 100 mL/min). CHN analyses were performed with a LECO CHNS-932 instrument. Field emission scanning electron microscopy (FE-SEM) images were obtained with an FEI NOVA NANOSEM 230 on uncoated as-made samples. For structure solution, synchrotron XRD data were collected in capillary mode (0.5 mm diameter) at the RIKEN materials science BL44B2 beamline at SPring-8, Japan, using a wavelength of 0.4995 Å.

Conformational Analysis. Conformational analysis of 2E134TMI was performed using the Conformers module of the Materials Studio suite of programs.[8] A systematic grid scan at one fixed step of the N(3)−C(2)−C(9)−C(10) torsion angle was followed by minimization using the cvff force field.[9] The energies of the conformers are given in kilocalories per mole relative to the energy of the most stable conformer. The molecular volumes, taken as the volume enclosed by the Connolly surface,[10] of several (stable or unstable) conformers of 2E134TMI were calculated using Materials Studio, with a Connolly radius of 1.4 Å, a van der Waals scale factor of 1, and an ultrafine grid resolution (0.15 Å intervals).

Optical Characterization. Mueller matrix measurements were made with a homemade Mueller matrix microscope constructed from a plasma light source (Thorlabs), a monochromator (Oriel), two linear polarizers (Thorlabs), two achromatic wave plate combinations (Thorlabs) working as rotating compensators, a sample holder, and

a Hamamatsu digital charge-coupled device (CCD). Further details are given in ref 11.

■ RESULTS AND DISCUSSION

Zeolite Synthesis. 2E134TMI was found to be a very poor SDA at 150 °C, yielding ill-crystallized products after prolonged heating (Table 1).

Table 1. Summary of Synthesis Results at 150 °C

H$_2$O/SiO$_2$	time (days)	product	H$_2$O/SiO$_2$	time (days)	product
3.3	6	amorphous	6.5	3	amorphous
	13	amorphous		13	amorphous
3.3	20	amorphous + HPM-1		30	amorphous + unknown
	23	amorphous + HPM-1	6.2	44	HPM-2
3.9	31	amorphous + unknown		78	HPM-2 + ITW

Under the most concentrated conditions (water/silica = 3.3), hydrothermal treatment for 20 and 23 days produced basically amorphous solids by XRD analysis. These contained however some weak peaks that were later identified as belonging to the new pure silica chiral zeolite HPM-1.[4] On the basis of peak areas in the 17−18.6° 2θ range, we estimate the relative crystallinities of these solids at around 10% and 12%, respectively. At slightly higher water/silica ratios we obtained signs of a crystalline phase (Figure S1, Supporting Information) after 30 days that may possibly be zeolite STF[12] and/or STF/SFF.[13] intergrowths. A very long heating treatment (44 days) afforded a material with an XRD pattern consisting of broad bands, designated as HPM-2, which is more conveniently synthesized at higher temperature (see below). This is a layered organosilicate, and its detailed characterization will be reported elsewhere. Still longer heating (78 days) produced the same material with traces of ITW.

The poor performance as an SDA of 2E134TMI was unexpected given the criteria proposed by Kubota et al. for good structure directors ("rigid, bulky and relatively short (<10 Å for the longest axis) molecules with moderate hydrophobicity are the best candidates for the structure-direction of new high-silica molecular sieves").[14] 2E134TMI qualifies. Compared to the imidazolium cations that we have previously studied, 2E134TMI is less rigid than 1,3-dimethylimidazolium (13DMI), 1,2,3-trimethylimidazolium (123TMI), and 1,3,4-trimethylimidazolium (134TMI),[7] but more rigid than 1-ethyl-2,3-dimethylimidazolium (1E23DMI),[15] all of which are selective for ITW. It is considerably more rigid than the unselective bisimidazolium and benzilimidazolium cations. 2E134TMI is also bulkier than our "good" imidazolium SDAs: its Connolly volume is 166.3 Å^3 for the most stable conformation and 165.6 Å^3 for the conformation found in STW, see below, which indicates 2E134TMI is around 15% larger than 1E23DMI. Its longest dimension, considering a van der Waals radius of 1.1 Å for H, is closely around the 10 Å mentioned by Kubota et al. (9.9 Å for the most stable conformation, 9.6 Å for the most unstable conformation, and 10.0 Å for the conformation found in the zeolite). Finally, its hydrophobicity is also moderate and similar to that of the "working" imidazolium SDAs as judged from the percentage of transfer of its iodide salt from a water solution to chloroform following the experimental procedure described by Kubota et

al.[14] (see below). Thus, we decided to give 2E134TMI a chance at a higher temperature.

By increasing the synthesis temperature to 175 °C, three crystalline phases were formed quickly (Table 2). From the

Table 2. Summary of Synthesis Results at 175 and 185 °C

H$_2$O/SiO$_2$	time (days)	product	H$_2$O/SiO$_2$	time (days)	product^f
3.3	13	HPM-1 (+ITW)	5.7	7	HPM-1
	23	HPM-1 (+ITW)		11	HPM-1 (+ITW)
3.8	2	HPM-1 + amorphous		39	ITW
4.0	3	HPM-1	5.9	21^b	HPM-2 + ITW
	5	HPM-1		32	ITW
	7	HPM-1	10	4	HPM-2
	12	HPM-1 (+ITW)		17	HPM-2 + dense^c
4.5	11	HPM-1		28	dense^c + HPM-2
	17	HPM-1 + ITW	10	3	amorphous + HPM-2
4.8^a	2	HPM-2		5	HPM-2
	5	HPM-2	3.8	3^{d,e}	HPM-1
	7	HPM-2		3^d	HPM-1
5.5	16	HPM-1			

^{a}Synthesis at 185 °C. ^{b}Synthesis using HPM-2 seeds obtained at 150 °C (1 wt % seeds, based on silica). ^{c}Tridymite-like dense phase. ^{d}Synthesis scaled by a factor of 5. ^{e}Synthesis using STW seeds obtained at a water/silica ratio of 4.0 (1 wt % seeds, based on silica). ^{f}Major products are listed first, trace products appear between parenthesis.

most concentrated solutions, the new silica zeolite HPM-1 (with the chiral framework type STW,[4] first reported as the silicogermanate SU-32)[6] crystallized in pure form in a relatively wide range of synthesis times (3−7 days at water/silica ratios of 4.0). The synthesis can be scaled up by at least a factor of 5. Reaction temperatures as high as 185 °C worked for low water/silica ratios (3.8). Under these conditions, at a slightly higher water/silica ratio (4.8), HPM-2 crystallizes instead. Prolonged heating at 175 °C transformed the STW zeolite into ITW, and the full characterization of this ITW material will be reported later. At higher water/silica ratios the crystallization is dominated by HPM-2 and ITW, with evidence of an in situ transformation of the former to the latter as the crystallization time is prolonged (system seeded with HPM-2). At the highest water/silica ratios tried (10), the transformation is to a dense tridymite-like phase. We found no signs of the ill-crystallized STF or STF/SFF phases obtained in some syntheses at 150 °C (Figure S1, Supporting Information; Table 1).

The dramatically different performance of 2E134TMI at 150 °C and at 175 °C contrasts with our experience in the synthesis of silica zeolites by the fluoride route, where increasing the

crystallization temperature in the 135−175 °C range most frequently produces a moderate increase in the crystallization rate.[16] From the limited amount of data in Tables 1 and 2, the overall crystallization of HPM-1 must be over 10 times faster at 175 °C than at 150 °C, which from the Arrhenius equation suggests an apparent activation energy over 140 kJ mol^{-1}.

The transfer from water to chloroform of 2E134TMI iodide is 21.6% (measured following the procedure by Kubota et al.),[14] indicating an intermediate hydrophilicity, very similar to those of other imidazolium cations able to produce zeolite ITW (it is in fact between the values found for 1E23DMI and 13DMI).[15] According to Kubota et al.,[14] an intermediate hydrophilicity may be necessary for organic cations to perform well as SDAs in the synthesis of high-silica zeolites by the hydroxide route, reflecting the compromise between a high solubility in water and interaction with the hydrophobic silica. For the fluoride synthesis, as proposed previously,[7] an intermediate hydrophilicity may help stabilize double four-membered ring (D4R) zeolites that would be strained for a pure silica composition but can be relaxed by host−guest interactions that polarize the Si−O bond.[17,18] Both STW and ITW have D4R units in their structures, and in fact, the proposed polarization effect helps explain how the STW zeolite can be synthesized as a SiO$_2$ framework despite lacking a so-called "flexibility window".[19] The flexibility window, i.e., the range of densities that a zeolite can display without stressing and deforming its tetrahedra, appears as an important property for "attainable" zeolites.[20] We have proposed that a broad flexibility window may enhance the chances that a favorable host−guest interaction is found, hence improving the probability that a zeolite is realized.[21] In the case of STW, the flexibility that the framework itself lacks might be provided by the Si−O bond polarization effect mentioned above.[4]

Physicochemical Characterization. The large difference in performance of 2E134TMI at 150 and 175 °C could be due to a degradation of the organic cation at the higher temperature, with a degradation product effectively acting as the SDA at 175 °C. In this regard, it is important to know if the organic cation is occluded intact within the STW zeolite. C/N chemical analysis, Table 3, suggests there are six species of cation-like composition occluded per cell of the STW framework (that is, full occupancy of the large $[4^6 5^8 8^2 10^2]$ cages). However, chemical analysis does not rule out degradation, especially as the measured ratio is somewhat lower than the stoichiometric expectation. The H/N ratio, by contrast, matches the theoretical value for 2E134TMI if no water or Si−OH connectivity defects exist. The lack of water in STW is supported by the thermogravimetric analysis (Figure S2, Supporting Information), which shows only around 0.2% weight changes below 250 °C. Significant weight loss only occurs between 400 and 600 °C.

To unambiguously check the integrity of 2E134TMI inside HPM-1, we performed ^{13}C MAS NMR on the as-made material (Figure 1, bottom). However, the spectrum shows only seven

Table 3. Chemical Analysis of As-Made STW Zeolite

[C] (%)	[H] (%)	[N] (%)	C/N^a	H/N^a	TG^b	unit cell composition^c
11.8	2.0	3.7	3.7 (4.0)	7.5 (7.5)	78.46 (78.79)	|C$_8$H$_{15}$N$_2$F|$_{6.1}$[SiO$_2$]$_{60}$

^{a}Molar ratios. Theoretical values for 2E134TMI are given in parentheses. ^{b}Residue (wt %) in the thermogravimetric analysis up to 1000 °C (the amount in parentheses corresponds to the SiO$_2$ content in the unit cell composition given in the last column). ^{c}SDA calculated from the N analysis assuming the SDA is intact, its charge is compensated by F, and the TG residue is SiO$_2$.
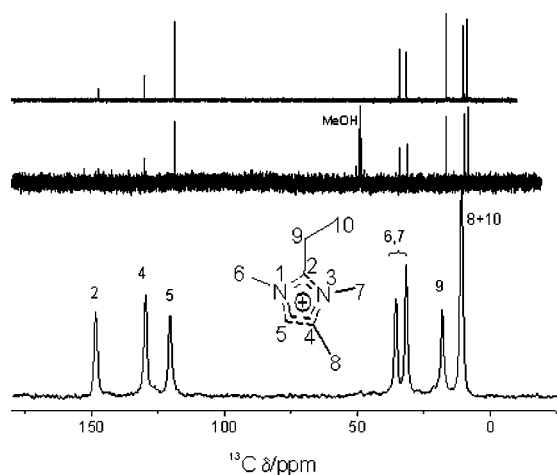
Figure 1. Solid-state ^{13}C MAS NMR spectrum of as-made 2E134TMI-STW (bottom) and ^{13}C NMR spectra in D_2O solution of the dissolved zeolite (middle; see the text, methanol added as a chemical shift reference) and of the pristine 2E134TMI iodide (top).

resonances, instead of eight, including those corresponding to the three C atoms in the imidazolium ring (115−150 ppm range), both methyls bonded to N (around 36 and 31 ppm), the secondary carbon of the ethyl group (around 18 ppm), and just one resonance at higher field instead of two for the two $\underline{C}H_3C$ carbons: the methyl substituent at C(4) of the imidazolium ring and the ethyl group. For this reason, we liberated the imidazolium cation by dissolving a small amount (∼0.06 g) of the as-made zeolite in HF (48% aqueous solution, 1.16 mL) and diluting the solution with 4 mL of D_2O. A drop of methanol was then added as a chemical shift reference. The ^{13}C and ^1H NMR in solution are shown in Figures 1 and 2, respectively, together with those of fresh 2E134TMI iodide in solution.
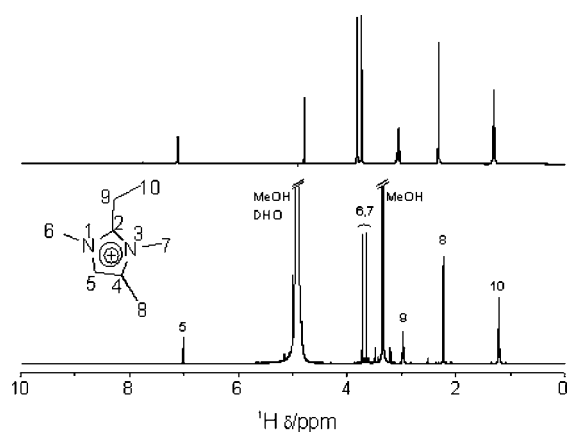

Figure 2. ^1H NMR spectra in D_2O solution of the dissolved 2E134TMI-STW zeolite (bottom) and of the pristine 2E134TMI iodide (top).

These spectra demonstrate the integrity of the occluded cation: the ^1H NMR spectrum features all the expected resonances with the correct multiplicities and relative intensities. Nonetheless, we note a small but noticeable ^1H chemical shift displacement when this spectrum is compared to the spectrum of the pristine iodide. This is likely a consequence of concentration and pH differences of the solutions compared.

For instance, the HDO/MeOH signal is shifted 0.11 ppm to lower field compared to its "normal" value. We found a similar shift in previous work[16] and ascribed it to an enhanced hydrogen bond in HF solution. In the ^{13}C NMR spectrum of the dissolved zeolite (Figure 1, middle), the high-field resonances of both methyl groups attached to carbon atoms are now clearly resolved, while, as in our previous report,[16] the imidazolium C(2) is not observed, a reasonable expectation due to its characteristically low relative intensity in this proton decoupled experiment. These experiments unambiguously demonstrate that 2E134TMI, and not a degradation product, is the actual organic SDA in the crystallization of HPM-1.

With regard to the SiO_2 framework itself, the ^{29}Si MAS NMR spectrum in Figure 3 shows two main resonances for the as-
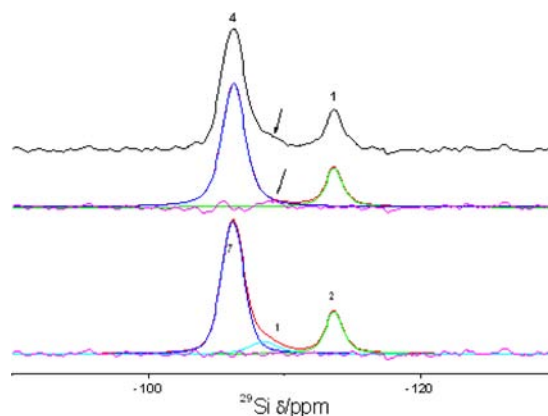

Figure 3. ^{29}Si MAS NMR spectrum of as-made 2E134TMI-STW (top). Two deconvolutions with two or three resonances are shown (with relative intensities of the deconvoluted components as indicated). The simulations also show a difference spectrum.

made material (four well-resolved resonances were found in the calcined product).[4] Deconvolution of the spectrum shows a 4:1 relative intensity for the resonances at −106 and −113 ppm, respectively. These are assigned to Si atoms in and out of the D4R, respectively, suggesting that there are 80% Si sites involved in the D4R (as is in fact the case in the STW topology). The chemical shift of −106 ppm is an outstandingly low-field resonance for a $Si[OSi]_4$ environment, suggesting very acute SiOSi average angles for the sites involved in the D4R in STW (around 139.5°, according to the empirical correlation of Thomas et al.).[22] Careful inspection of the spectrum reveals an asymmetry at the high-field side of the −106 ppm resonance. A deconvolution with three resonances yields relative intensities close to 7:1:2 that may suggest a symmetry lowering from $P6_122/P6_522$ to $P6_1/P6_5$. Finally, the lack of resonances around −102 ppm or beyond −120 ppm suggests the absence of Si−O−Si connectivity defects and of a Si coordination number larger than four,[23] respectively.

The tetrahedral coordination of Si in this F-containing, as-made material is characteristic of silica zeolites with fluoride occluded in the D4R, where no direct covalent bonding between F and Si exists. The ^{19}F MAS NMR spectrum (Figure S3, Supporting Information) reveals a prominent resonance at −35.7 ppm which, despite being at an exceedingly low field, is close to the typical −38 to −40 ppm characteristic of F$^-$ in a siliceous D4R.[24]

The organics and fluoride can be removed by calcination in air at 700 °C for 3 h. The microporosity of the silica (Figure S4,

Supporting Information) is revealed by its type I N_2 adsorption isotherm,[25] and the pore size distribution obtained by the Horvath−Kawazoe method shows openings of around 5 Å (Figure S5, Supporting Information),[26] in good agreement with the size of the 10-membered ring (10MR) limiting access through the helicoidal channels (5.5 × 5.8 Å as determined from the reported structure; a second set of smaller channels, 8MR, 3.2 × 4.5 Å, run normal to the main pore).[4]

The morphology of HPM-1 crystallites varies between micrometer-sized well-faceted hexagonal prisms terminated by pyramids at both ends ("double pencil" shape) to larger pod-shaped particles apparently composed of smaller crystallites, Figure 4. The latter morphology seems to be favored for long crystallization times and at higher H_2O/SiO_2 ratios and may be related to partial dissolution and recrystallization processes.

Structural Characterization. The structure of as-made HPM-1 was refined using the GSAS program[27] with the EXPGUI graphical interface[28] in space group $P6_122$. We started with a model of the SiO_2 framework derived from the structure
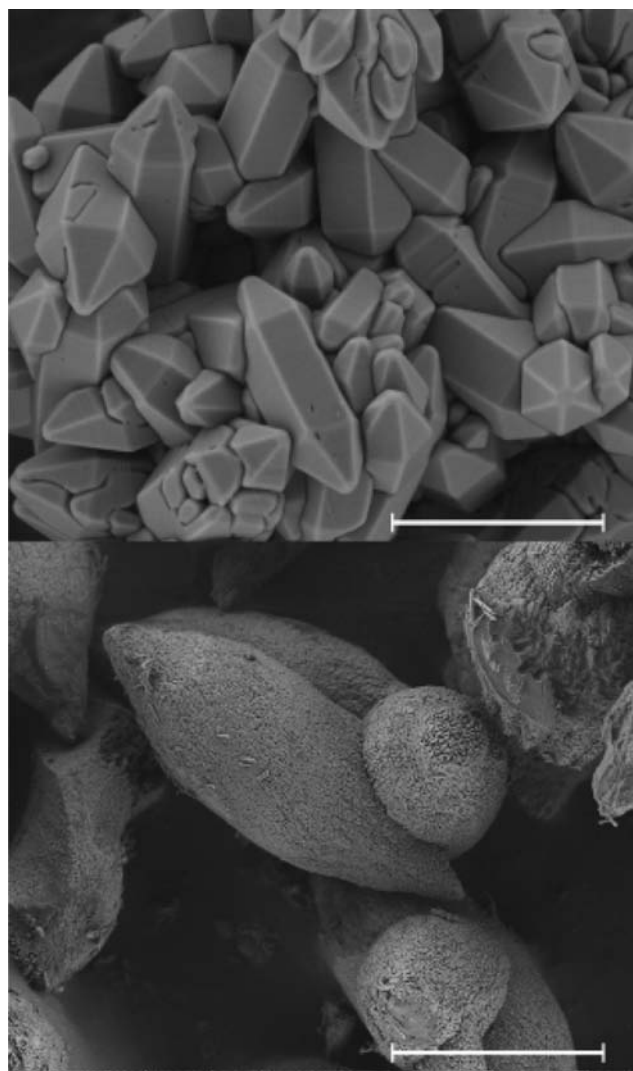

Figure 4. FE-SEM pictures of as-made HPM-1 showing two typical yet distinct morphologies: bipyramidal hexagonal rods (crystallized at H_2O/SiO_2 = 4, for 5 days, top, scale bar 2 μm) and podlike aggregates (H_2O/SiO_2 = 5.5, 16 days, bottom, scale bar 10 μm). Both materials were synthesized at 175 °C.

of the calcined material but using the cell parameters of the as-made zeolite (a = 11.90 Å, c = 29.686 Å) and including the fluoride atoms in the center of the D4R cages, in agreement with the ^{19}F MAS NMR spectrum (Figure S3, Supporting Information). The organic cation was introduced as the assembly of two rigid bodies: (1) the main imidazolium with three methyl groups and (2) the ethyl group as a satellite able to freely rotate around the C(2)−C(9) bond. Fractional occupancies of 0.5 were used to yield a final occupancy of 1 cation per cage, in agreement with the chemical analysis in Table 3. Details of the refinement, including a CIF file and the Rietveld plot, are given as Supporting Information.

The imidazolium ring was treated as a rigid body in the refinement, but there were no other geometric constraints. The SiOSi angles averaged for each Si site are grouped around two values: sites involved in the D4R show more acute angles (142.3 ± 2.51°) than the sites not involved (154.6°), justifying the two main resonances resolved in the ^{29}Si MAS NMR spectrum (calculated chemical shifts of −107.3 ± 1.4 and −115.0 ppm, respectively, Table S2, Supporting Information). The cation is located in the large cavities with the imidazolium ring lying approximately on the {100} family of planes (Figure 5). The ethyl group is out of the plane by ∼126° (measured as the N(3)−C(2)−C(9)−C(10) dihedral angle) and points roughly toward an 8MR window. The two symmetrical orientations found in each cavity (with half-occupancy each) have their imidazolium rings almost coplanar, but rotated and slightly displaced, so that two methyl groups of one are almost coincident with two methyl groups of the other, while the third methyl substituent of one is almost coincident with the C(2)−C(9) bond of the other. The unsubstituted position of the aromatic ring, C(5), and its symmetric partner are apparently 0.47 Å apart, a consequence of the disorder.

Interestingly, the conformation found for 2E134TMI in HPM-1 is 2 kJ mol^{-1} less stable (Figure S7, Supporting Information) than the most stable conformation calculated in vacuum by molecular simulations (about). There may be a significant contribution of the conformational energy to the global energetics of the crystallization. Conversely, the conformation found in HPM-1 appears to be well bound by the silica framework itself. As seen in Figure 6, the C end of the ethyl group is close to three of the oxygen atoms in the 8MR window and the distances (not shown) between the methyl substituent at position 4 of the imidazolium ring and some framework oxygen atoms are as low as 3.31 and 3.34 Å (for (C(8)···O(7) and C(8)···O(3), respectively). This "locked" conformation shall also bear a significant entropic cost to the crystallization of HPM-1. Furthermore, the distance between ethyl groups (3.36 Å) in adjacent cages through the 8MR window indicates a shortened contact, as defined by Zefirov.[29] This may suggest only one of the symmetrical orientations is realized, as the resulting closest distance between cations (in that case through ethyl−methyl fragments) in adjacent cavities would increase to a more comfortable 4.42 Å distance. This would imply a symmetry lowering to $P6_1/P6_5$ that may find support in the ^{29}Si MAS NMR results shown above (Figure 3). Unfortunately, attempts to refine the structure in $P6_1/P6_5$ failed, likely due to the large number of parameters involved.

Other conformations have energy similar to that found by refinement where the ethyl group is similarly offset from the imidazolium plane. Those with the ethyl group closer to N(3) (with torsion angles of around −54° and +54°) have been ruled out on the basis of a Rietveld refinement (see the Supporting
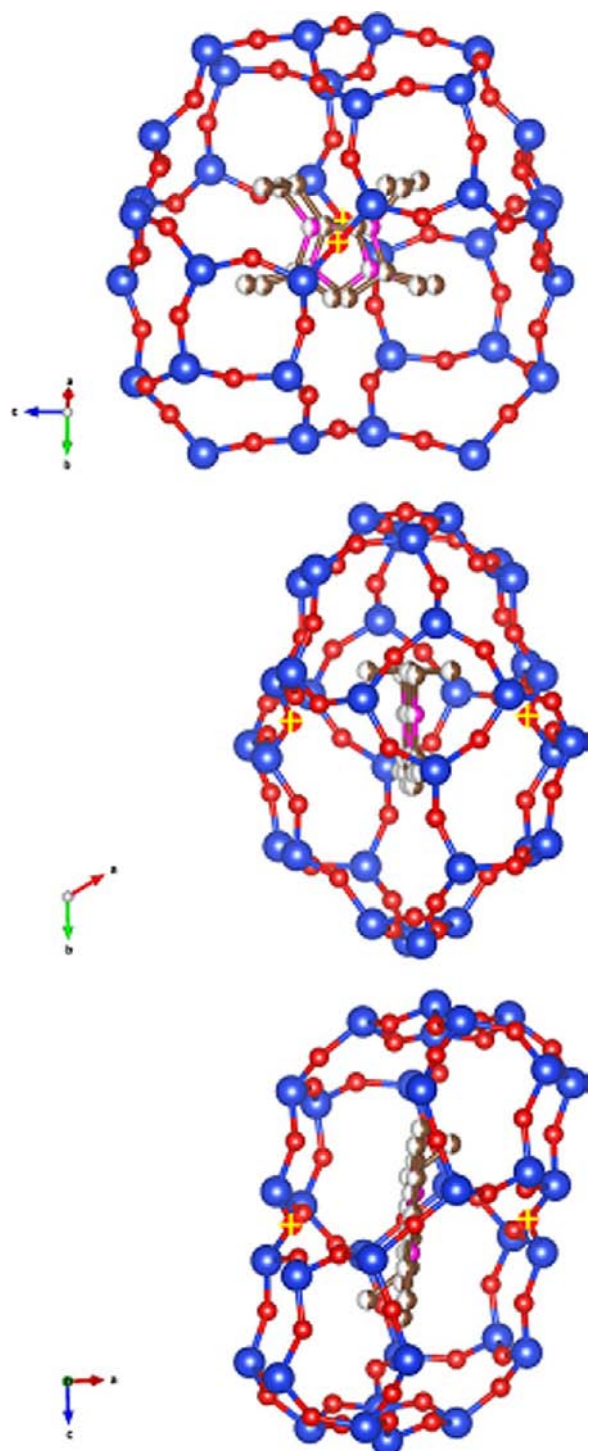
Figure 6. Closest O−C distances (Å) between the O of the 8MR window and the −CH₃ end of the ethyl substituent of 2E134TMI.

Figure 5. Three views along the directions specified by the arrows of the large [4⁶5⁸8²10²] cavity of HPM-1, containing the 2E134TMI cation. Two symmetrical orientations of the cation are shown. In each view, two O(2) atoms defining the minimum thickness of the cavity across the imidazolium ring are marked with a yellow cross (blue, silicon; red, oxygen; white/brown, C; white/pink, N).

Information). The one with the ethyl group at −126° would correspond to the P6₅22 structure. Obviously, the conformations with positive rotation of the ethyl group are mirror images of the ones with the same but negative rotation angle. The energy of the conformers with 0° and 180° in vacuum is not high enough to prevent interconversion, so there is no
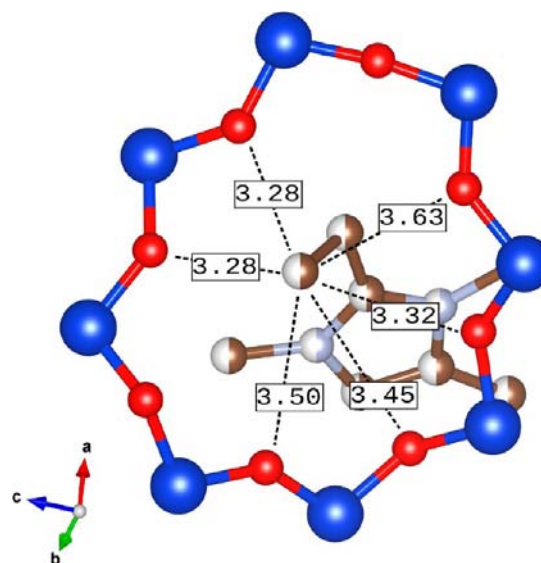
atropisomerism in vacuum. However, the conformation in the zeolite is effectively locked, so the cations in P6₁22 and P6₅22 could be considered pseudoatropisomers.

The STW-type framework has a large concentration of D4R units, with four-fifths of the silicon sites belonging to such a unit. According to prior reports,[7] zeolite structures containing a D4R are strained for a silica composition. In fact, molecular mechanics calculations predicted STW could not be crystallized as SiO₂.[30] Furthermore, the lack of a "flexibility window" in STW added to this unlikelihood.[19] However, as we have proposed in our preliminary paper,[4] the flexibility of the STW framework may be increased in its as-made uncalcined form by host−guest interactions between the silica framework, the fluoride, and organic ions (with an intermediate hydrophilicity). This has been demonstrated for ITW zeolites, where polarization of the Si−O bond translates into less rigid tetrahedra.[7] Our crystallographic data quantify the deviation of tetrahedrality in as-made STW as 3.4° (calculated as the standard deviation of the O−Si−O angles from the regular tetrahedral angle of 109.5°). This value is comparable to those found for as-made ITW synthesized with several cations (3.6−4.7°).[16] This deviation from tetrahedrality supports the idea that in HPM-1 the crystallization of a silica material containing a D4R also is made attainable by the proposed flexibility enhancement brought about by polarization of the Si−O bond. Also, HPM-1 undergoes a small but noticeable framework expansion upon calcination (0.8%) that suggests the flexibility enhancement in the as-made material allows the framework to shrink, maximizing host−guest contacts. For instance, the [4⁶5⁸8²10²] cavity has 4.24 Å of free space across the imidazolium ring (measured between O(2) atoms; see Figure 5) in the as-made material, and this distance increases to 4.38 Å in the calcined zeolite.

On the other hand, we note that during this study we found no signs of the crystallization of an SOF-type zeolite, despite the strong competition of this zeolite with STW under germanium-based compositions using diisopropylamine as an SDA.[6] Both types of zeolites can be described as "built from the same building layer",[6] both contain a D4R, and both have similar framework densities, while SOF does have the flexibility

window that STW lacks.[19] Clearly, the additional stabilization by host−guest interactions that the silica system requires can be achieved with 2E134TMI and F in STW but not in SOF.

Optical Characterization. Enantioselectivy is of great importance in the production of bioactive molecules (drugs, pesticides, and food additives) since more often than not each enantiomer displays a different activity. With its current silica composition, HPM-1 has no catalytic activity but could be nonetheless used in adsorption/separation processes for the resolution of racemic mixtures. For instance, the common herbicide mecoprop is commercialized as a racemic mixture despite the fact that only the R isomer displays herbicidal activity.[31] Additionally, introduction of catalytic sites (e.g., Al, Ti, Sn, ...) should be possible. A chiral titanium silicate should show potential, for instance, for enantiomeric epoxidations. However, profiting from the chirality of the helicoidal channel of HPM-1 in enantioselective physicochemical or chemical processes would require producing homochiral material (or, alternatively, blocking the channels of a given hand).[32] To monitor the progress of any synthetic strategy aimed at producing homochiral solids, one needs to unambiguously determine the enantiomeric excess. For a microcrystalline powder that is not composed of soluble chiral molecules, this issue is far from trivial. Single-crystal diffraction can make use of the Flack parameter to ascertain the absolute configuration of a single crystal.[33] However, even if microdiffraction on very small crystallites is affordable, determining the enantiomeric excess of a microcrystalline solid with any confidence would require the analysis of a large number of crystals. On the other hand, if enantiomorphs had distinct habits, a simple Pasteur-like resolution with a light microscope could establish enantiomeric excess. This is not the case with HPM-1 (Figure 4).

Chemical (catalysis) and physicochemical (adsorption) tests may also be troublesome for a number of reasons, including the following: the external surface of the crystallites may behave nonspecifically, the selection of a suitable probe molecule (with the proper size and shape not only to enter the pores but also to behave differently in helical pores of different hand) is not straightforward, and enantioselectivity may be sensitive to the conditions. For instance, in a molecular simulation of the adsorption of 1,2-dimethylcyclobutane in each of the helical pores of UCSB-7K (a gallium germanate which presents pores of both hands in each unit cell), Clark et al. found that the significant selectivities calculated at low partial pressure and loading levels decayed to zero when approaching saturation.[32]

An optical assay of chirality would be much faster presuming the chiral zeolite displays a measurable optical activity. The optical determination of the chirality of a transparent material can be made by measurement of circular birefringence (CB). CB is twice the angle of optical rotation, i.e., the azimuthal rotation of linearly polarized light as it propagates through the material. While this is routinely performed for small molecules in solution or isotropic solids, the measurements of CB in an anisotropic (linearly birefringent) direction of a crystal are much more demanding. We have experience in these measurements using Mueller matrix polarimetry. Mueller matrix polarimetry analyzes the polarization properties of a sample in terms of the transformation of an input Stokes vector (S_{in}) via the Mueller matrix (M): $S_{out} = MS_{in}$. S_{out} is the output Stokes vector. We have used this technique, for example, to measure the complete gyration tensor of quartz.[34,35]

For small (micrometer-sized) and as-grown crystals without parallelepiped morphologies, CB measurements are even more

difficult. The optical characterization of such samples is better achieved using Mueller matrix microscopy (MMM). MMM generates 16 magnified images of the sample, each representing one of the elements of the 4×4 Mueller matrix expressed in terms of measurable input and output polarization state intensities. However, one practical limitation is that Mueller matrix polarimeters with the highest sensitivity are based on designs that are not compatible with CCD detectors because they use photoelastic modulators with extremely high speeds of polarization modulation.[36] An alternative design for an imaging instrument that allows high spatial resolution is to implement a Mueller matrix microscope based on a dual rotation compensator setup.[11,37] Briefly, it consists of a crossed polarizer microscope with two rotating compensators added before and after the sample that act as a complete polarization state generator (PSG) and polarization state analyzer (PSA) pair. By collecting images as a function of rotations of the PSA and PSG, the M of a sample at each pixel can be solved through pseudoinversion.

For an anisotropic crystal, the 16 images of M are not simply related to the fundamental optical parameters of interest in this study, CB. To achieve a separation of the convolution of optical properties, we use an analytic inversion algorithm.[38] As a result of this inversion method, three basic optical parameters are obtained: circular birefringence (CB), horizontal linear birefringence (LB), and 45° linear birefringence (LB′). Their corresponding absorbing partners (CD, LD, LD′) vanish because HPM-1 zeolite is transparent in the visible part of the electromagnetic spectrum. Given an orientation, CB is the essential parameter to distinguish the handedness of the microcrystal. For a material within zeroth order of birefringence (total birefringence between $+\pi$ and $-\pi$), the CB value obtained by this method is a quantitative measurement of twice the optical rotation. However, when performing microscopy, it is usual to study samples with variable thickness, in which the order of birefringence varies from crystal to crystal. For birefringent materials with multiple orders of birefringence, the CB value obtained by this method needs to be corrected according to order-corrected total birefringence (TB):

$$CB_{order\text{-}corrected} = CB \frac{TB_{order\text{-}corrected}}{TB} \quad (1)$$

where $TB = (CB^2 + LB^2 + LB'^2)^{1/2}$, taking values between 0 and π and $TB_{order\text{-}corrected} = TB + 2\pi n$. n is the order of birefringence. Only by knowing the value of n can the meaningful value $CB_{order\text{-}corrected}$ be recovered. Order changes are signaled by strong discontinuities in the birefringence of neighbor pixels.

For practical purposes, we selected a sample that contains large crystals of zeolite HPM-1 (roughly 30 μm $\times$ 70 μm) together with smaller crystals (around 10 μm) of ITW (see Figure S8, Supporting Information). This sample was synthesized at 175 °C for 12 days at $H_2O/SiO_2 = 4.0$ (seventh entry in Table 2). Crystallites were collected with a fine paintbrush and then dispersed on a drop of index-matching oil (Richard-Allan Scientific Resolve high-viscosity immersion oil, refractive index 1.515) deposited on a glass slide. The index-matching oil greatly enhanced the transmission of light through the crystals, permitting light to transverse areas not bound by parallel planes normal to the direction of incidence. After the sample preparation, most of the zeolites of the bipyramidal rod form shown in Figure 4a were sitting flat on the microscope slide (Figure 7). For all MMM measurements the transmitted

light was propagating normal to the major axis of the zeolite crystallites.
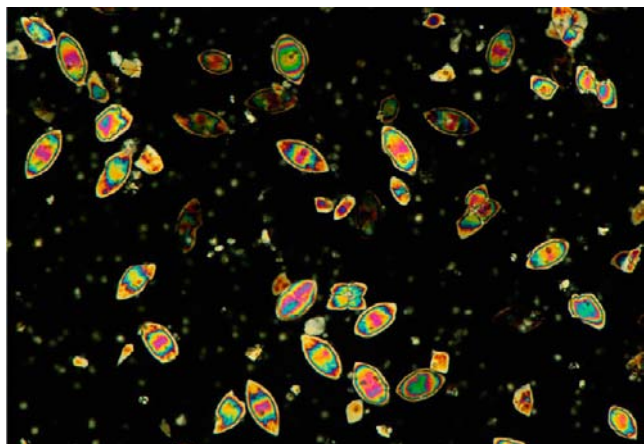

Figure 7. HPM-1 zeolite dispersed in index-matching oil and examined in a microscope under crossed polarizers (smaller crystallites correspond to zeolite ITW).

Figure 8 shows the measured LB and LB′ for two differently oriented HPM-1 crystallites. Clearly, the crystallite on the left,
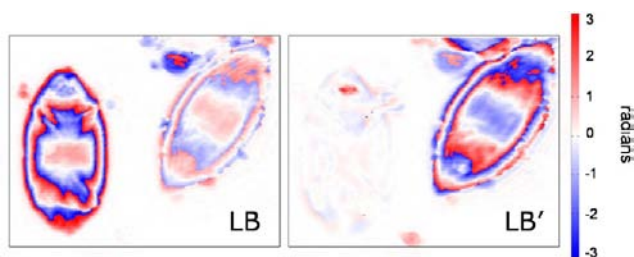

Figure 8. Horizontal linear birefringence (LB) and 45° linear birefringence (LB′) as determined from the Mueller matrix measured at 500 nm for two crystallites with different orientations. The discontinuities in sign (sharp red to blue transitions) are due to changes in the order of birefringence.

oriented vertically, has strong LB and almost zero LB′, while for the tilted crystallite on the right LB′ dominates. The c-axis is the direction that contains the two pyramid edges. The discontinuities in sign (sharp red to blue transitions in the image) are due to changes in the order of birefringence, most likely coming from variations in the crystallite thickness. These sign changes should not be interpreted as a variation of the orientation of the optic axis. In fact, the only parts of the image that allow a straightforward quantitative analysis are the borders of the crystal, especially at the pyramidal edges, where the crystal is thin enough to maintain zeroth-order TB. The vertically oriented zeolite of Figure 8 has positive (red) LB in the borders, meaning that the refractive index in the vertical direction (n_y) is higher than in the horizontal direction (n_x), as LB = $2\pi(n_x - n_y)L/\lambda$. Therefore, we can deduce that the zeolite has a negative birefringence because along the c-axis the refractive index is lower than in the orthogonal directions.

The $P6_122/P6_522$ space group of chiral HPM-1 has two independent components of the optical activity tensor, **g**, that can contribute to the measured CB depending on the crystal orientation. **g** takes the form

$$\mathbf{g} = \begin{bmatrix} g_{11} & 0 & 0 \\ 0 & g_{11} & 0 \\ 0 & 0 & g_{33} \end{bmatrix}$$

$$(2)$$

g_{33} is the only contributing element when light is propagating along the optic axis, and g_{11} is the only term when the direction of propagation of light is perpendicular to the c-axis. The latter was the orientation of all crystallites we have measured, and according to the classical link between CB and the optical rotation tensor,[39] the measured CB for these orientations should be simply given by CB = $2\pi g_{11}/\lambda n$, where n is the average refractive index and λ the wavelength. In this crystallographic direction CB is only a minor contribution to the TB measured in the zeolite. In Figure 9a the imaged CB for
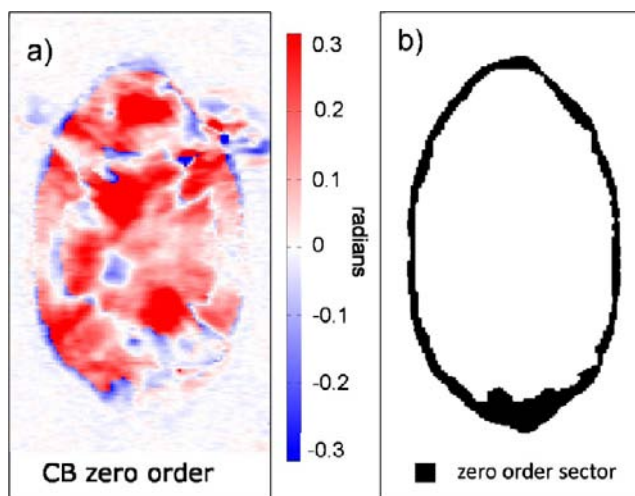

Figure 9. Zeroth-order CB (a) of a single HPM-1 crystallite. The zeroth-order calculation applies to the narrow black ring shown in (b) and to the background of the image. These are areas where the total birefringence of the sample stays between $+\pi$ and $-\pi$. Inner parts of the crystallite (predominantly in red in (a)) have higher orders of birefringence due to the increased thickness. In these parts CB cannot be directly taken from (a).

the vertical crystallite of Figure 8 shows predominantly positive values (red) through most of the crystal image, but this result is based on the unrealistic assumption of zeroth-order birefringence everywhere. In fact, and as discussed above, only a narrow ring at the edge of the zeolite (Figure 9b) remains zeroth order, and in this part of Figure 9a, CB is negative (blue). For higher orders of birefringence, present in the inner parts of the zeolite image, we expected more sign changes in CB as happens in the LB of Figure 8, but transitions beyond first order could not be observed in CB, probably due to the limited sensitivity offered by an instrument that relies on mechanical light modulation. Nevertheless, from the results of Figure 9, the crystallite has negative CB in directions perpendicular to the optic axis.

Not enough crystallites where measured to offer a statistically significant general picture of the chirality. Among six valid measurements, four of them showed negative CB as in Figure 9 and two others were equivocal. The approach described here will be applied in the future, using a Mueller matrix microscope with increased sensitivity, for a systematic characterization of the enantiomeric form of this chiral zeolite.

11982

dx.doi.org/10.1021/ja405088c | *J. Am. Chem. Soc.* 2013, 135, 11975−11984

CONCLUSIONS

The performance of 2E134TMI as an SDA in the synthesis of pure silica zeolites by the fluoride route is quite poor at 150 °C and much more effective at 175 °C. At that temperature two different crystalline phases (HPM-1 and HPM-2) are obtained at relatively short crystallization times. The phase selectivity is controlled by the water content of the reaction. After prolonged heating, both phases can transform to ITW or, for relatively dilute compositions, to a tridymite-like dense phase.

As-made HPM-1 contains intact 2E134TMI cations in its relatively large $[4^6 5^8 8^2 10^2]$ cavities, somehow locked in a relatively unstable conformation by interaction with framework oxygen. The calculated deviation from tetrahedrality of its SiO_4 tetrahedra and the expansion of the framework upon calcination support the idea that enhanced framework flexibility attributed to a polarization of the Si−O bond by host−guest interactions makes this framework attainable for crystallization of a composition that would otherwise be too strained.

A preliminary investigation of the optical activity of HPM-1 by Mueller matrix microscopy shows that the circular birefringence of a single crystallite is measurable. This technique may constitute the basis of a method for determining the overall chirality of a sample with statistical significance. We deem this is a necessary tool for undertaking a systematic investigation aimed at the crystallization of a purely homochiral zeolite.

ASSOCIATED CONTENT

ⓢ Supporting Information

Powder XRD data for two solids obtained at 150 °C, thermogravimetric analysis and ^{19}F MAS NMR of as-made HPM-1, N_2 adsorption−desorption isotherm and Horvath−Kawazoe plot of calcined HPM-1, details of Rietveld refinement, Rietveld plot, crystallographic and structural parameters for as-made HPM-1 (full crystallographic data also provided as a CIF file), experimental and calculated ^{29}Si chemical shifts for as-made HPM-1, conformational plot in vacuum of 2E134TMI, and FESEM picture of the sample characterized by MMM. This material is available free of charge via the Internet at http://pubs.acs.org.

AUTHOR INFORMATION

Corresponding Author
macamblor@icmm.csic.es

Present Address
∥A.R.: Universidad Autónoma Metropolitana, campus Iztapalapa, UAM-I, San Rafael Atlixco, 186 Vicentina, 09340 Mexico City, Mexico.

Notes
The authors declare the following competing financial interest(s): A.R. and M.A.C. have filed a Spanish patent application on the material studied in this paper.

ACKNOWLEDGMENTS

REFERENCES

(1) Treacy, M. M. J.; Newsam, J. M. *Nature* **1988**, *332*, 249. Newsam, J. M.; Treacy, M. M. J.; Koetsier, W. T.; de Gruyter, C. B. *Proc. R. Soc. London, Ser. A* **1988**, *420*, 375.

(2) Dryzun, C.; Mastai, Y.; Shvalb, A.; Avnir, D. *J. Mater. Chem.* **2009**, *19*, 2062.

(3) Davis, M. E.; Lobo, R. F. *Chem. Mater.* **1992**, *4*, 756.

(4) Rojas, A.; Camblor, M. A. *Angew. Chem., Int. Ed.* **2012**, *51*, 3854.

(5) Baerlocher Ch.; McCusker, L. B. Database of Zeolite Structures. http://www.iza-structure.org/databases/, accessed on March 22, 2013.

(6) Tang, L.; Shi, L.; Bonneau, C.; Sun, J.; Yue, H.; Ojuva, A.; Lee, B. L.; Kritikos, M.; Bell, R. G.; Bacsik, Z.; Mink, J.; Zou, X. *Nat. Mater.* **2008**, *7*, 381.

(7) Rojas, A.; Martínez-Morales, E.; Zicovich-Wilson, C. M; Camblor, M. A. *J. Am. Chem. Soc.* **2012**, *134*, 2255.

(8) *Materials Studio 6.0*; Accelrys Inc.: San Diego, CA, 2011.

(9) Dauger-Osguthorpe, P.; Roberts, V. A.; Osguthorpe, D. J.; Wolff, J.; Genest, M.; Hagler, A. T. *Proteins: Struct., Funct., Genet.* **1988**, *4*, 21.

(10) Connolly, M. L. *J. Appl. Crystallogr.* **1983**, *16*, 548.

(11) Freudenthal, J.; Hollis, E.; Kahr, B. *Chirality* **2009**, *21* (S1), S20.

(12) Wagner, P.; Nakagawa, Y.; Lee, G. S.; Davis, M. E.; Elomari, S.; Medrud, R. C.; Zones, S. I. *J. Am. Chem. Soc.* **2000**, *122*, 263.

(13) Villaescusa, L. A.; Zhou, W.; Morris, R. E.; Barrett, P. A. *J. Mater. Chem.* **2004**, *14*, 1982.

(14) Kubota, Y.; Helmkamp, M. M.; Zones, S. I.; Davis, M. E. *Microporous Mater.* **1996**, *6*, 213.

(15) Rojas, A.; San Román, M. L.; Zicovich-Wilson, C. M.; Camblor, M. A. *Chem. Mater.* **2013**, *25*, 729.

(16) Villaescusa, L. A. Ph.D. Thesis, Universidad Politécnica de Valencia, 1999.

(17) Zicovich-Wilson, C. M.; San-Román, M. L.; Camblor, M. A.; Pascale, F.; Durand-Niconoff, J. S. *J. Am. Chem. Soc.* **2007**, *129*, 11512.

(18) Zicovich-Wilson, C. M.; Gándara, F.; Monge, A.; Camblor, M. A. *J. Am. Chem. Soc.* **2010**, *132*, 3461.

(19) Kapko, V.; Dawson, C.; Treacy, M. M. J.; Thorpe, M. F. *Phys. Chem. Chem. Phys.* **2010**, *12*, 8531.

(20) Sartbaeva, A.; Wells, S. A.; Treacy, M. M. J.; Thorpe, M. F. *Nat. Mater.* **2006**, *5*, 962.

(21) Medina, M. E.; Platero-Prats, A. E.; Snejko, N.; Rojas, A.; Monge, A.; Gándara, F.; Gutiérrez-Puebla, E.; Camblor, M. A. *Adv. Mater.* **2011**, *23*, 5283.

(22) Thomas, J. M.; Klinowski, J.; Ramdas, S.; Hunter, B. K.; Tennakoon, D. T. B. *Chem. Phys. Lett.* **1983**, *102*, 158.

(23) Koller, H.; Wolker, A.; Villaescusa, L. A.; Díaz-Cabañas, M. J.; Valencia, S.; Camblor, M. A. *J. Am. Chem. Soc.* **1999**, *121*, 3368.

(24) Camblor, M. A.; Barrett, P. A.; Díaz-Cabañas, M. J.; Villaescusa, L. A.; Puche, M.; Boix, T.; Pérez, E.; Koller, H. *Microporous Mesoporous Mater.* **2001**, *48*, 11.

(25) Sing, K. S. W.; Everett, D. H.; W. Haul, R. A.; Moscou, L.; Pierotti, R. A.; Rouquerol, J.; Siemieniewska, T. *Pure Appl. Chem.* **1985**, *57*, 603.

(26) Horvath, G.; Kawazoe, K. *J. Chem. Eng. Jpn.* **1983**, *16*, 470.

(27) Larson, A. C.; Von Dreele, R. B. *General Structure Analysis System (GSAS)*; Los Alamos National Laboratory Report LAUR 86-748; Los Alamos National Laboratory: Los Alamos, NM, 1994.

(28) Toby, B. H. *J. Appl. Crystallogr.* **2001**, *34*, 210.

(29) Zefirov, Yu. V. *Crystallogr. Rep.* **1997**, *42*, 865.

(30) Sastre, G.; Corma, A. *J. Phys. Chem. C* **2010**, *114*, 1667.

(31) Zipper, C.; Nickel, K.; Angst, W.; Kohler, H.-P. E. *Appl. Environ. Microb.* **1996**, *62*, 4318.

(32) Clark, L. A.; Chempath, S.; Snurr, R. Q. *Langmuir* **2005**, *21*, 2267.

(33) Flack, H. D.; Bernardinelli, G. *Chirality* **2008**, *20*, 681.

(34) Arteaga, O.; Canillas, A.; Jellison, J. *Appl. Opt.* **2009**, *48*, 5307.

(35) Arteaga, O.; Freudenthal, J.; Kahr, B. *J. Appl. Crystallogr.* **2012**, *45*, 279.

(36) Arteaga, O.; Freudenthal, J.; Wang, B.; Kahr, B. *Appl. Opt.* **2012**, *51*, 6805.

(37) Kahr, B.; Freudenthal, J.; Gunn, E. *Acc. Chem. Res.* **2010**, *43*, 684.

(38) Arteaga, O.; Canillas, A. *Opt. Lett.* **2010**, *35*, 559.

(39) Nye, J. F. *Physical Properties of Crystals: Their Representation by Tensors and Matrices*; Oxford University Press: New York, 1985.